CrossMark

RESEARCH ARTICLE

Flow and acoustic characteristics of non-axisymmetric jets at subsonic conditions

Puja Upadhyay[1] · Griffin Valentich[1] · Rajan Kumar[1] · Farrukh Alvi[1]

Abstract Flow and acoustic behavior of two asymmetric, rectangular (AR = 4) and elliptic (AR = 2.5), jets are studied and compared to an equivalent area round jet. The jets are operated at a Mach number of 0.9 and temperature ratio of 1. Time-averaged flow field measurements are carried out using planar and stereoscopic particle image velocimetry. In addition, far-field microphone measurements are performed to compare jet acoustics. Mean flow field results demonstrate that for the given Mach number and aspect ratios, rectangular and elliptic jet properties are somewhat modified compared to the round jet. The elliptic jet exhibits properties that are intermediate between two geometric extremes. Moderately enhanced mixing in asymmetric jets as a result of weak streamwise vortices is evidenced by overall shorter potential core, faster centerline velocity decay, and higher shear layer growth rates. Centerline turbulence levels and transverse shear stress distribution also show enhanced fluctuations for non-circular jets. Compared to their major axis planes, relatively higher turbulence levels are measured in the minor axis planes for both rectangular and elliptic jets. Far-field acoustic measurements reveal the asymmetric nature of the sound field. Compared to the round jet, major axis orientation for asymmetric jets is observed to provide moderate acoustic benefit in the downstream direction. However, enhanced fluctuations in the minor axis plane result in a marginal noise augmentation at moderate to high frequencies in this plane for downstream polar angles.

1 Introduction

Non-circular nozzle geometries are used in variety of applications, such as combustion control, reacting flows, aircraft propulsion, and heat transfer (Gutmark and Grinstein 1999). In most cases, the use of non-axisymmetric geometries is primarily motivated by the potential to obtain enhanced entrainment and increase mixing between the jet and its surroundings. Reduction in growth rate due to compressibility effects further necessitates alternative geometries for efficient mixing of shear flows in high-speed applications, such as supersonic combustion (Papamoschou and Roshko 1988). In modern day, high-performance aircraft, rectangular nozzle geometry, among others have been of particular interest. This non-circular geometry facilitates the implementation of thrust vectoring and thrust reversal to increase overall maneuverability and agility (Capone 1975; Hiley et al. 1976). Moreover, mixing efficiency of asymmetric nozzle shapes is also explored as passive control methods in efforts to reduce jet plume or infrared signature, and potentially attenuate radiated noise (Seiner and Ponton 1992; Veltin and McLaughlin 2009; Viswanath et al. 2016). Rectangular geometries are also being explored as possible nozzle concepts for high-speed civilian aircrafts (Bridges 2012; Bridges and Wernet 2015).

Even though there have been a notable number of studies dedicated to the investigation of asymmetric jet properties, these studies are still sparse compared to a large volume of

✉ Puja Upadhyay
  pujaupadhyay@gmail.com

[1] Department of Mechanical Engineering, Florida State University, FAMU-FSU College of Engineering, 2003 Levy Ave, Tallahassee, FL 32310, USA

theoretical and experimental data available for axisymmetric turbulent jets. Experimental studies involving comparisons of flow and acoustic properties for different nozzle geometries at high-speed, shock-free conditions are especially lacking. Some of the early work investigating non-circular jets involved measurement of bulk flow field properties (Sforza et al. 1966; Trentacoste and Sforza 1968). It was reported that three dimensional jets (such as, rectangular and elliptic) consist of three regions of centerline velocity decay, namely, potential core, characteristic (two-dimensional), and axisymmetric. The characteristic decay region begins when the shear layers bounding the short sides of the jet meet. In the axisymmetric decay region, the jet achieves similarity in both major and minor axis planes, thus approaching axisymmetry. The existence and relative extent of these regions mainly depend on nozzle geometry and aspect ratio (AR) (Sfeir 1979). Subsequently, many other investigations were performed to understand the flow dynamics of rectangular (Krothapalli et al. 1981; Tsuchiya and Horikoshi 1986; Quinn 1994), elliptic (Ho and Gutmark 1987; Hussain and Husain 1989; Husain and Hussain 1993) and other jet configurations (Zaman 1996, 1999; Kim and Samimy 1999).

In addition to enhanced mixing capabilities of these jets, a very interesting phenomena known as axis-switching was reported by these studies. Axis-switching occurs when the minor axis plane (shorter dimension) grows faster compared to the major axis (longer dimension) and, at some location downstream, the jet axes interchange. This process of axis-switching is also known to be one of the main underlying mechanism for vigorous entrainment in asymmetric jets. Krothapalli et al. (1981), Tsuchiya and Horikoshi (1986), Ho and Gutmark (1987), Hussain and Husain (1989) and Quinn (1994) are a few, among others, who have demonstrated axis-switching in elliptic and rectangular jets. In contrast, Zaman (1999), Kinzie and McLaughlin (1999), Valentich et al. (2016), and few others exhibited cases where this phenomenon was absent. Some of these studies also reported lower entrainment rates. Several authors have analyzed mechanisms associated with axis-switching and discussed critical effects initial conditions, nozzle aspect ratio, and existing vortex dynamics have on the deformation of jet cross section (Husain and Hussain 1993; Zaman 1996; Grinstein 2001). In rectangular and elliptic jets, self-induced motion due to non-uniform curvature of spanwise vortex rings is believed to be the main mechanism for enhanced transport of momentum and axis-switching (Ho and Gutmark 1987; Hussain and Husain 1989; Grinstein 2001). However, this dynamics of coherent spanwise vorticity is shown to be more profound under natural (screech) or artificial excitation. When excited, these spanwise structures are more organized, intensified, and go through a series of contortions (Hussain and Husain 1989). In non-excited jets, especially at high speeds, these spanwise structures occur at random, lack organization, and

hence axis-switching may be delayed or not occur altogether (Zaman 1996). Furthermore, axis-switching is also influenced by the presence of streamwise vortices due to upstream secondary flow. The strength and orientation (sense of rotation) of these vortices can either favor or resist axis-switching. For instance, Zaman (1999) demonstrated a high-subsonic rectangular jet with two counter-rotating vortex pairs orientated in an 'out-flow' sense. Here, the outward induced velocity of the vortex pairs further stretched the jet in the major axis, hence resisting axis-switch. Streamwise vortex dynamics can be further strengthened by strategic placement of tabs or trailing edge modifications, prompting rapid axis-switch and more vigorous entrainment (Zaman 1994; Kim and Samimy 1999).

Rapid mixing of the jet plume promoted by asymmetric nozzle geometry can potentially reduce the length of high-turbulence, noise producing region, resulting in attenuation of radiated noise. However, the number of jet noise studies undertaken to investigate the effectiveness of these nozzles in reducing turbulent mixing noise is fairly limited. Acoustic studies at supersonic jet speeds have shown that non-axisymmetric nature of sound radiated from these nozzles results in 'loud' and 'quiet' planes, where the 'loud' plane could potentially be directed away from noise sensitive directions (Seiner and Ponton 1992; Kinzie and McLaughlin 1999; Goss et al. 2009). In these studies, the minor axis plane is generally observed to be louder than major axis in the peak noise radiation direction. Spectral comparisons revealed enhanced high-frequency noise in the minor axis plane compared to the major. For high subsonic speeds, Tam and Zaman (2000) argued that radiated noise field from elliptic and large AR rectangular jets was fairly axisymmetric and showed agreement with similarity spectra for supersonic circular noise data of Tam et al. (1996). Alternatively, some others have demonstrated azimuthal variation of the radiated noise even at high-subsonic speeds. Coles (1959) compared acoustic field of rectangular slot nozzles with AR = 14 and 100 to an equivalent area round jet using a full-scale turbojet engine. Appreciable reduction of 3 dB in total sound power was attained with the higher AR nozzle. Bridges (2012) compared acoustic results from three converging rectangular nozzles (AR = 2, 4, 8), showing an increase in azimuthal dependence of overall sound pressure level (OASPL) with aspect ratio. Moreover, spectral comparisons with an equivalent area round jet in the aft direction revealed that the rectangular jet (AR = 8) results in decrease of low-frequency peak noise and an increase in noise levels at high frequencies in the minor axis plane. Studies of Morris and Bhat (1995), Kinzie (1995), and Kinzie and McLaughlin (1999) demonstrated higher noise levels in the minor axis plane is due to the higher growth rate of flapping mode that radiates primarily in this plane. Shih et al. (1992) also analyzed instability modes of a moderate aspect ratio rectangular jet

at various Mach numbers. His study showed that all Mach numbers except for $0.6 \leq M \leq 0.85$ exhibit anti-symmetric mode. For $0.6 \leq M \leq 0.85$, existence of both symmetric and anti-symmetric modes with a constant switch between the two was observed.

The study presented is a part of an on-going research at Florida State University (FSU) on the viability of asymmetric nozzles in future aircraft designs. The overall goal of this project is to understand the effect of nozzle exit geometry on flow and acoustic characteristics of high-speed jets at various Mach numbers and temperature conditions. The objective of the present investigation is to provide comprehensive flow field and noise measurements for two asymmetric, rectangular (AR = 4) and elliptic (AR = 2.5), jets at a high-subsonic condition. An equivalent area round nozzle is used as a baseline case to study the effect of nozzle exit geometry on jet properties. The jets are operated at isothermal conditions (temperature ratio of 1) and a Mach number of 0.9 ($Re_D \approx 5 \times 10^5$). Time averaged flow measurements are acquired using planar and stereoscopic particle image velocimetry (PIV). The impact of nozzle exit geometry in the noise characteristics of the jet are assessed using far-field acoustic measurements. Results from flow measurements are used to compare time averaged properties, such as growth of shear layer, production of streamwise structures, turbulence distribution, and so on, between the asymmetric and round jets. Moreover, far-field acoustic results reveal effects of nozzle asymmetry on the radiated sound field. Overall, comprehensive experimental results presented in this paper will be a valuable contribution to the scarce database of asymmetric jets at high subsonic conditions. Moreover, these experimental results will also serve as a benchmark for future CFD simulations of high-subsonic rectangular and elliptic jets.

2 Experimental setup and measurements

2.1 Test facilities

The experiments for this study were performed in two high-speed jet facilities housed in the Florida Center for Advanced Aero-propulsion (FCAAP) at FSU. Flow field measurements were conducted in the Short Take Off Vertical Landing (STOVL) facility. This is a blow-down jet facility which can simulate flow induced effects in both impinging and free jet configurations. The room housing the jet facility (5.5 m × 7.3 m × 9 m) is not anechoic, but sufficiently large to allow for proper entrainment and jet development. The facility is capable of attaining Mach numbers and temperature ratios (T_o/T_{amb}) up to 2.2 and 2.3, respectively. More details on facility operations and capabilities can be found in Valentich (2016).

Far-field acoustic measurements were conducted in the anechoic chamber of the High-Temperature Jet Facility (HotJet) at FCAAP. Similar to STOVL, the HotJet is a blow-down facility that allows the study of free as well as impinging jets. The primary difference is that HotJet employs a Sudden Expansion (SUE) ethylene pipe burner to attain realistic jet exhaust temperatures. The facility is capable of generating air speeds up to Mach 2.6 and stagnation temperatures up to 1500 K. The jet exhausts into a fully anechoic chamber (5 m × 5.7 m × 4.3 m) that simulates a free-field environment for measuring far-field acoustics. The cut-off frequency of the chamber is approximately 300 Hz. Detailed information on facility design, hardware, and operational capabilities is discussed by Craft et al. (2016).

2.2 Nozzle geometries and test conditions

This study uses three converging nozzles with rectangular, elliptic, and round exit geometries. All nozzles have an equivalent diameter, D_{eq}, of 2.54 cm and begin contraction from a 5.72 cm inner diameter pipe. The overall length of the round and elliptic nozzles is 11.9 cm, while the rectangular is 11.4 cm. The rectangular and elliptic nozzles are manufactured using electrical discharge machining (EDM) which provides a smooth transition from the circular pipe to the respective exit geometry. The lip thickness for each nozzle is approximately 0.75 mm. The contraction of each nozzle (in both axes for asymmetric nozzles) is designed using a fifth-order polynomial for parallel inlet and exit flow.

The origin for the jet exhaust flow is chosen to be at the center of the nozzle exit plane with the x-axis oriented perpendicular to this plane in the streamwise direction, y-axis oriented along the minor axis, and z-axis oriented along the major axis. Images of each nozzle's exit geometry and the coordinate system (axis orientation) for this study can be seen in Fig. 1.

For the experiments presented, the nozzles shown in Fig. 1 are operated at a nozzle pressure ratio (NPR = P_o/P_{amb}) of 1.69 and temperature ratio (TR = T_o/T_{amb}) of 1, nominally. Here, the subscripts, o and amb, correspond to stagnation and ambient conditions, respectively. For these conditions, the exit Mach number of the jet is $M_j \approx 0.9$.

Since two different test rigs (see Sect. 2.1) were used for measurement of flow and acoustic properties, care was taken to maintain same upstream pressure and temperature conditions in both test facilities. First, the use of the same nozzles in both facilities ensures that there are no geometric scaling effects. Moreover, the same nozzle inlet pipe sizes and set of flow conditioning devices were used upstream of the nozzle in both setup. The flow conditioning
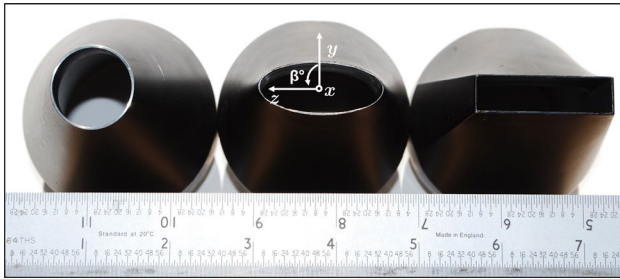
Fig. 1 Image of nozzle exit geometry (*left to right-round*, *elliptic*, and *rectangular*). All nozzles have an equivalent diameter of 2.54 cm. The rectangular and elliptic nozzles have an aspect ratio of 4 and 2.5, respectively. The coordinate system for this study is overlaid on the elliptic nozzle exit plane. The x axis is oriented in the streamwise, y in the minor axis, and z in the major axis direction

unit consisted of a stainless steel honeycomb and a combination of fine and coarse wire meshes. The relative placement of these flow conditioning devices and their upstream location, as measured from the nozzle exit, was maintained to be the same in both facilities. In addition, upstream jet conditions were precisely controlled, monitored, and documented for all the runs in both jet facilities (see Sect. 2.4).

2.3 Measurement techniques

2.3.1 Particle image velocimetry (PIV)

The spatial evolution of jet flow field from three different nozzle geometries was studied using both planar and stereoscopic PIV. The main jet was seeded with glycol droplets approximately 0.5 μm generated using a Laskin seeder. The ambient was seeded with Rosco fog fluid (1–5 μm) using a Rosco fog machine. A double pulsed Nd-Yag laser (Evergreen HP, 380 mJ) was used to illuminate the

region of interest in the flow field. A 10 mm laser beam is focused using a spherical lens and passed through a cylindrical lens to obtain a sheet wide enough to cover the flow region of interest. Laser sheet thickness of approximately 1.5 and 3 mm was used for planar and stereoscopic PIV, respectively. The cameras and the laser are triggered using a LaVision programmable timing unit (PTU) connected to a computer. The images were processed using Davis 8.2 software. For each case, a total of 1000 image pairs were processed using multipass algorithm with a final interrogation window size of 24×24 (Fig. 2).

Planar PIV was performed in the central plane of the jet in the streamwise direction spanning a total axial distance of $12D_{eq}$. For rectangular and elliptical nozzles, central planes along both major and minor axes were measured. Major axis PIV measurements were obtained by rotating the nozzle 90°, where the laser sheet passed through the central plane of the jet along the long axis (z-direction). A 4 Megapixel Imager Pro X CCD camera (2048×2048) was used to acquire images at a rate of 7.26 Hz. The time lag between two laser pulses was maintained at $dt = 4$μs to obtain particle displacements of 10–12 pixels in the jet core.

Stereoscopic or three component PIV (SPIV) was used to visualize select cross sectional planes of the jet, x/D_{eq} = 1, 2, 3, 5, and 8. Stereo PIV setup consisted of two 5.5 Megapixel sCMOS cameras (2560×2160) equipped with 105 mm Nikon lenses, providing a spatial resolution of approximately 0.5 mm. A stereo view of the laser sheet was obtained by placing two cameras, where the angle between the optical axes of two lenses was approximately 70°. 1000 image pairs were recorded at a rate of 10 Hz in double pulsed mode. A δt of 2.6 μs was used.

Fig. 2 Schematic showing top view of **a** planar PIV **b** stereoscopic PIV setup. The position of the laser sheet for both planar and stereoscopic configurations are denoted in the schematic
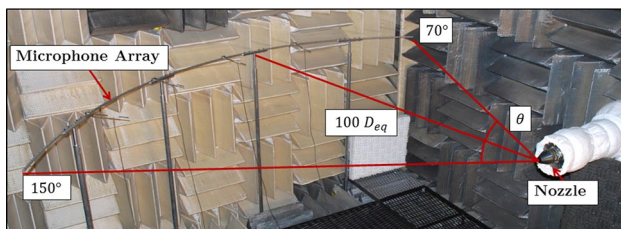

(a)   **(b)**
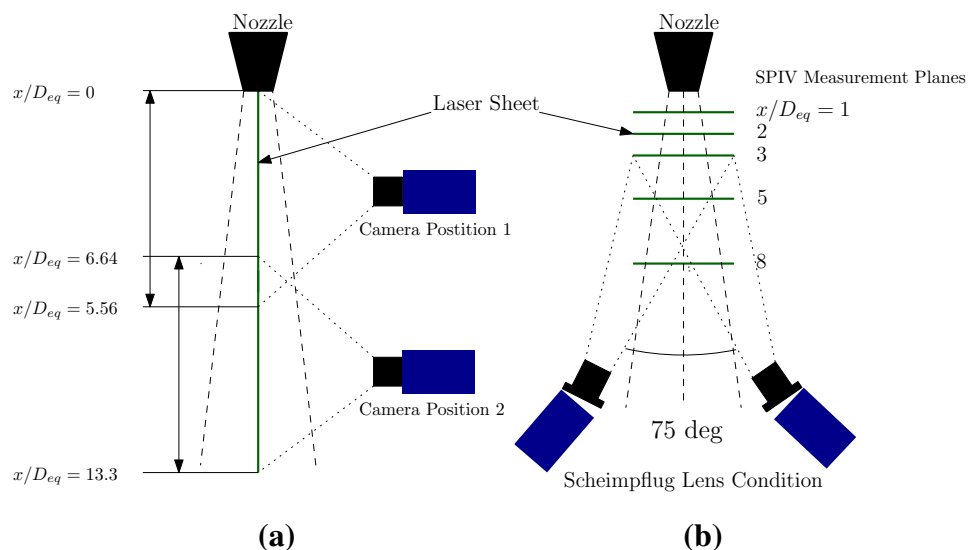
2.3.2 Acoustic measurements

Far-field acoustic measurements were performed using a circular arc of microphones placed at a radial distance of $100D_{eq}$ measured from the jet exit. The arc consisted of nine microphones placed every 10° between 70° and 150°, as measured from the jet inlet axis. Figure 3 shows the relative orientation of the jet and the microphones in the anechoic chamber. Acoustic measurements were performed using B&K 4939 free-field condenser microphones equipped with B&K 2670 preamplifiers and powered by a B&K model 2690 Nexus amplifier. The microphones are capable of measuring frequencies between 4 Hz and 100 kHz. To avoid aliasing, the signals were filtered through Stanford Research Systems SR-640 filter at 40 kHz. Data were acquired using National Instruments™ PXI-6133 14-bit, 16-channel simultaneously sampling system and a PC running LABVIEW software. The signals were sampled at 100 kHz for about 5 s. Narrow-band microphone spectra were obtained using an FFT length of 4096 samples with a Hanning window and 75% overlap.

For the non-axisymmetric nozzles, measurement of acoustic fields in both the axes was accomplished by rotating the nozzle 90° just as in the case of streamwise PIV measurements. The 'minor axis' acoustic measurements will describe results obtained when the microphone array lies in the minor axis plane (*xy* plane, $z = 0$) of the jet. Similarly, the 'major axis' acoustic measurements will have the microphone arc in the major axis plane (*xz* plane, $y = 0$).

2.4 Measurement uncertainty

The plenum pressure in STOVL facility was measured using an Omega PX-315 pressure transducer with a maximum error of 0.25% of the full scale, yielding a full-scale error value of 0.25 psi. Jet stagnation pressure in the HotJet facility was measured using an OMEGA (PX01C1-300AI), high-accuracy pressure transducer with a maximum full-scale error of 0.05%. This yields a full-scale error of 0.15 psi in the stagnation pressure measurements. In both the facilities, NPR fluctuations due to valve operation were limited to ±0.01. Hence, the maximum uncertainty in Mach number due to instrumentation and valve operation was approximately 1.1%. The total temperature in the stagnation chamber was measured with OMEGA K- and C-type thermocouples in the STOVL and HotJet facilities, respectively. Ambient temperatures in both the facilities were measured using K-type thermocouples. The maximum uncertainties for K- and C-type thermocouples provided by the manufacturer are 2.2 and 4 °C, respectively. Moreover, since the flow was not heated, temperature ratio of the jet fluctuated between 0.96 and 1. This introduced a maximum error of 4% in temperature measurement.

The velocity fields studied here are unknown prior to conducting PIV measurements. This conundrum of induced error due to particle size, particle lag, and number of samples acquired is difficult to estimate. To minimize the errors that could be associated with these properties, very small tracer particles ($\mathcal{O}(1\,\mu m)$) were used to reduce the particle lag in areas of large gradients. In addition, a large number of image pairs (1000) were acquired. Previous experiments have shown that, even in supersonic flows, results from PIV agree very well with velocities obtained from probe measurements (Alkislar et al. 2003). Although a very good agreement is expected, error in the velocity calculation was determined with the component uncertainty function included in DaVis 8.2. The regions of largest error, as expected, was found to be in the shear layers. In streamwise PIV, the maximum error in the velocity magnitude was found to be 1.5% of the fully expanded jet velocity, or 4.35 m/s. The error in the calculation of the magnitude of standard deviation of velocity for this case was determined to be 4% of U_j. From SPIV, cross plane velocity field at $x/D_{eq} = 2$ gave a maximum error of 0.6 and 0.86 % of U_j for in-plane and out of plane velocities, respectively. These error values are representative of all stereo planes acquired. Further details on the procedure used to determine PIV uncertainties can be found in Wieneke (2015). Finally, the error associated in the placement of the microphones is less than 1° in the polar angle and the uncertainty in the OASPL measurement is ± 0.5 dB.

Fig. 3 Experimental setup for far-field acoustic measurements showing the jet and circular arc of microphones in the anechoic chamber

3 Mean flow properties

As discussed in Sect. 1, research interest in non-circular nozzles is driven primarily due to higher entrainment and enhanced mixing capabilities of asymmetric jets. Various physical mechanisms at play, such as, jet perimeter stretching, production and distribution of streamwise vortices, dynamics of spanwise vorticity, and so on, affect jet mixing. In this section, we examine some pertinent time averaged flow properties for the given asymmetric jets and

compare these to the baseline results from an equivalent area circular nozzle.

3.1 Average shear layer properties

Figure 4 presents average streamwise velocity distribution in the jet central plane, measured using planar PIV. Here, the velocity values are normalized using the isentropic jet exit velocity (U_j), and the streamwise and spanwise distances are normalized using the equivalent diameter of the nozzles, D_{eq}. For non-axisymmetric nozzles, velocity distribution in the central plane for both major and minor axes is presented. In addition, contour line denoting values that are equal to $0.95U_j$ is overlaid on the velocity fields. A qualitative evaluation of these contour plots indicate that the flow fields for rectangular and elliptic jets are somewhat modified when compared to an equivalent area round jet. The most noticeable changes are observed in case of jet potential core length and shear layer spreading. Here, the rectangular jet appears to have the shortest, whereas the round jet appears to exhibit the longest potential core. Moreover, it can be observed that both asymmetric jets spread more in
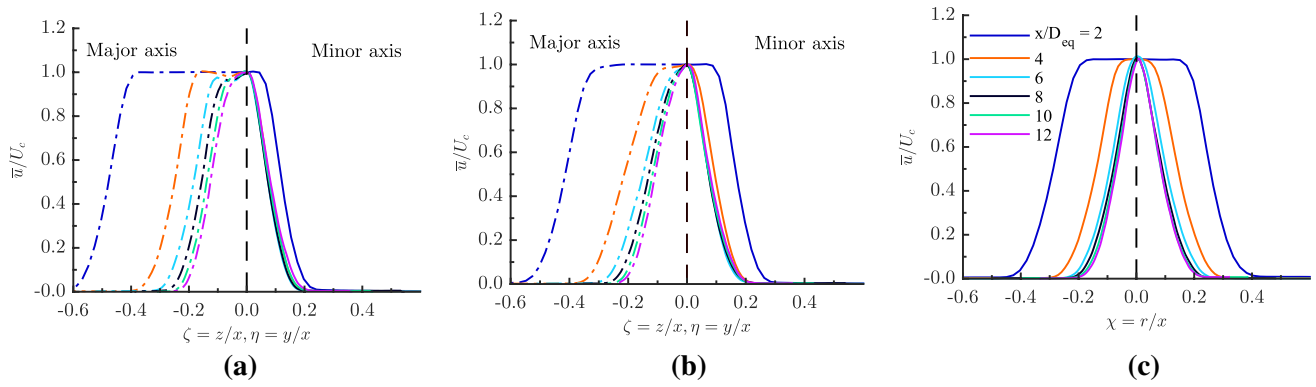
the minor axis plane compared to the corresponding major axis plane as well as the round jet.

Figure 5 presents mean streamwise velocity profiles at axial stations of $x/D_{eq} = 2, 4, 6, 8, 10$, and 12 for all three jets. Velocity values at each axial location (x) are non-dimensionalized using the corresponding centerline velocity values, U_c, at that location. For the asymmetric jets, velocity profiles in both major (xz plane, $y = 0$) and minor (xy plane, $z = 0$) axis half planes are presented in the same plot. Moreover, both spanwise (z) and transverse (y) distances from the nozzle exit are normalized using corresponding streamwise (x) locations. Here, non-dimensional variables $\eta = y/x$ and $\zeta = z/x$ for the minor and major axes, respectively, are used. For the round jet, non-dimensional variable $\chi = r/x$ is used.

Non-dimensional velocity profiles for both rectangular and elliptic jets reveal that for any given streamwise location, the width of the jet in the major axis plane is larger compared to the minor axis. This clearly shows that both asymmetric jets have not undergone axis-switching for the given measurement domain. Moreover, velocity profiles in the minor axis plane become geometrically similar for $x > 3D_{eq}$ and $x > 4D_{eq}$ for the rectangular and elliptic

Fig. 4 Colored contour plots showing time average streamwise velocity distribution, $\bar{u}/U_j$, in the jet central plane. The jets were operated at $M = 0.9$ for all three nozzles. For the asymmetric jets, velocity distribution in both major and minor axis planes is presented


(a) Rectanagular jet minor axis

(b) Rectangular jet major axis

(c) Elliptic jet minor axis

(d) Elliptic jet major axis
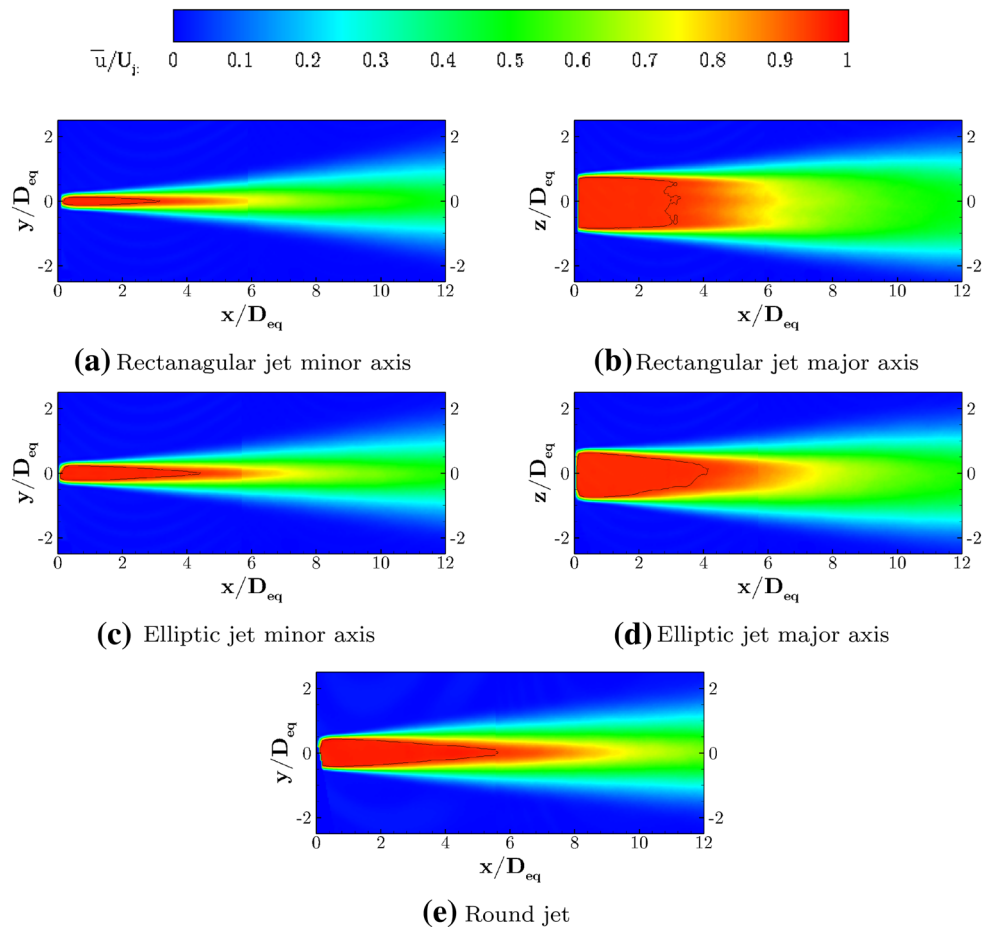
(e) Round jet

Fig. 5 Normalized mean streamwise velocity profiles at various axial locations for **a** *rectangular* **b** *elliptic* **c** *round* jets. For asymmetric jets, profiles in the major and minor axis planes are included in the same plot

jets, respectively. These locations appear to coincide with the collapse of potential core regions for these jets (see Fig. 6). Furthermore, these geometrically similar profiles in the minor axis plane also approach self-similar profiles of the equivalent area round jet for $x/D_{eq} > 8$ (see Fig. 5c). Similarly, velocity profiles in the major axis plane for both rectangular and elliptic jets begin to collapse for $x > 8D_{eq}$. However, despite this geometric similarity, these profiles are not identical to the profiles in the minor axis plane. This suggests that the jets are still evolving and have not yet approached axisymmetric state. Finally, the equivalent area round jet appears to achieve self-similarity for $x > 6D_{eq}$.

Next, to better examine the differences in jet spreading, distribution of quantities such as centerline velocity, jet half-width, and shear layer thicknesses will be analyzed for all three nozzle geometries. Figure 6 presents normalized centerline velocity values for rectangular, elliptic, and round jets, respectively. Centerline velocity values give a measure of the potential core of the jet and its rate of decay has been traditionally used as one of the means to estimate jet mixing and spreading. Current measurements

show that the potential core lengths for rectangular, elliptic, and round nozzles are approximately $3.3D_{eq}$, $4.5D_{eq}$, and $5.4D_{eq}$, respectively. This faster breakdown of the jet potential core in case of non-axisymmetric jets suggests enhanced mixing of the jet plume and faster spreading in comparison to the round jet. Moreover, for these nozzles, two distinct regions of centerline velocity decay are observed, denoted as R_2 and R_3 in the figures. These two decay rates are presumably associated with regions where the jet begins to assume geometric similarity in the minor and major axis planes. As seen in these figures, the decay rate for R_2 is higher in both rectangular ($m_2 = 0.072$) and elliptic ($m_2 = 0.074$) jets. For downstream region (R_3), the decay rates drop by as much as 50% for both rectangular ($m_3 = 0.033$) and elliptic ($m_3 = 0.039$) jet flow fields.

As discussed in Sect. 1, asymmetric jets are known to exhibit two distinct regions of centerline velocity decay, namely, characteristic and axisymmetric decay. Characteristic decay occurs when the jet becomes similar in the minor axis plane, whereas an axisymmetric type decay occurs when the jet is similar in both the axes and tends
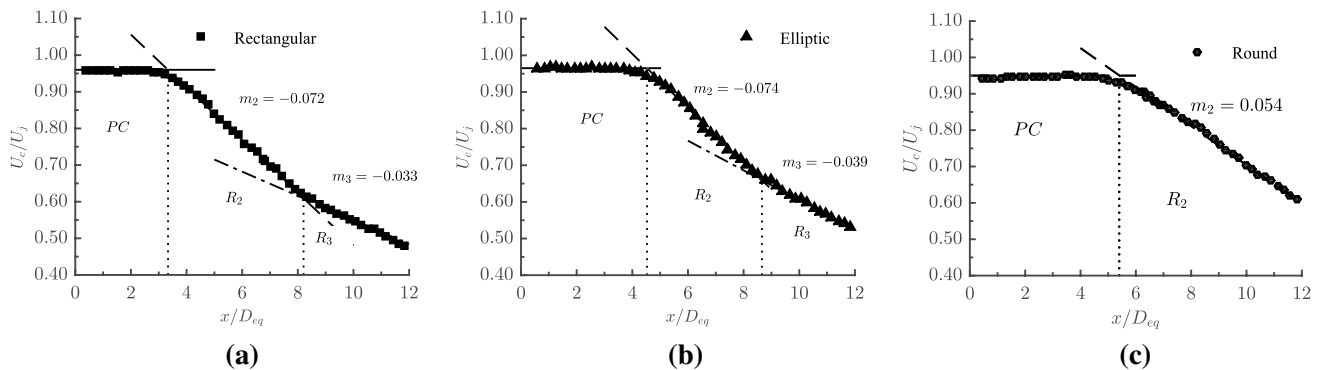

Fig. 6 Velocity distribution showing decay of mean streamwise velocity in the jet centerline for **a** *rectangular* **b** *elliptic* **c** *round* jets. The potential core region is denoted by PC. R_2 and R_3 denote two regions of centerline velocity decay

to axisymmetry (Sforza et al. 1966; Sfeir 1976, 1979; Krothapalli et al. 1981). However, as demonstrated in the context of Fig. 5, the rectangular and elliptic jets have not evolved to an axisymmetric state for the given measurement domain. This suggests that the decay observed in R_2 can be best classified as characteristic or two-dimensional. On the other hand, decay rates in R_3, which can be attributed to the jets approaching geometric similarity in the major axis plane, cannot be strictly classified as axisymmetric for the given measurement domain. The jets, however, are likely to achieve axisymmetry far downstream.

Finally, the round nozzle exhibits single region of decay for centerline velocity ($m_2 = 0.054$), where this overall rate appears to be approximately an average of regions R_2 and R_3 for non-axisymmetric jets. In summary, rectangular and elliptic jets have potential core lengths that are approximately 39 and 17%, respectively, shorter compared to the round jet. Moreover, for region R_2, centerline velocity decay rates for the rectangular and elliptical jets are 33 and 37%, respectively, higher compared to the round jet. On the other hand, the decay rates are approximately 39 and 28% lower for rectangular and elliptic jets, respectively, in R_3. It is evident from the results that asymmetric jets exhibit shorter potential core and a higher rate of centerline velocity decay, indicating enhanced mixing of the jet plume; a characteristic that may be utilized in modern day tactical aircraft to reduce infrared signature for improved stealth capabilities.

Further examining the spreading characteristics for the given nozzle geometries, jet half-width is plotted as a function of streamwise distance from the nozzle exit (see Fig. 7). Similar to centerline velocity distribution, jet half-width is used to estimate jet spreading or mixing, and is defined as the location where streamwise velocity is 50% of the local centerline velocity ($u = 0.5U_c(x)$). For the asymmetric nozzles, jet half-widths are denoted as $y_{0.50}$ (or b_y) and $z_{0.50}$ (or b_z) in the minor and major axis planes, respectively. For the round jet, $r_{0.50}$ (or b_r) denotes jet half-width in the radial axis. Slopes for jet half-width curves, denoting their growth rates, for all the nozzles are listed in their respective plots in Fig. 7. In addition, for a more comprehensive examination, the growth of low- and high-speed sides of shear layers is plotted in the same figure as the jet half-width for respective nozzles. The high-speed side of the shear layer corresponds to locations $((z/y/r)_{0.90})$, where the streamwise velocity is 90% of the local centerline velocity ($u = 0.9U_c(x)$). Similarly, the low-speed side corresponds to locations $((z/y/r)_{0.10})$, where $u = 0.1U_c(x)$.

For rectangular and elliptic jets, as seen in Fig. 7a and b, jet half-width curve exhibits continuous outward growth in the xy (minor axis) plane. The major axis plane, on the other hand, shows half-width distribution that is neither monotonic nor purely linear. For near nozzle locations, b_z
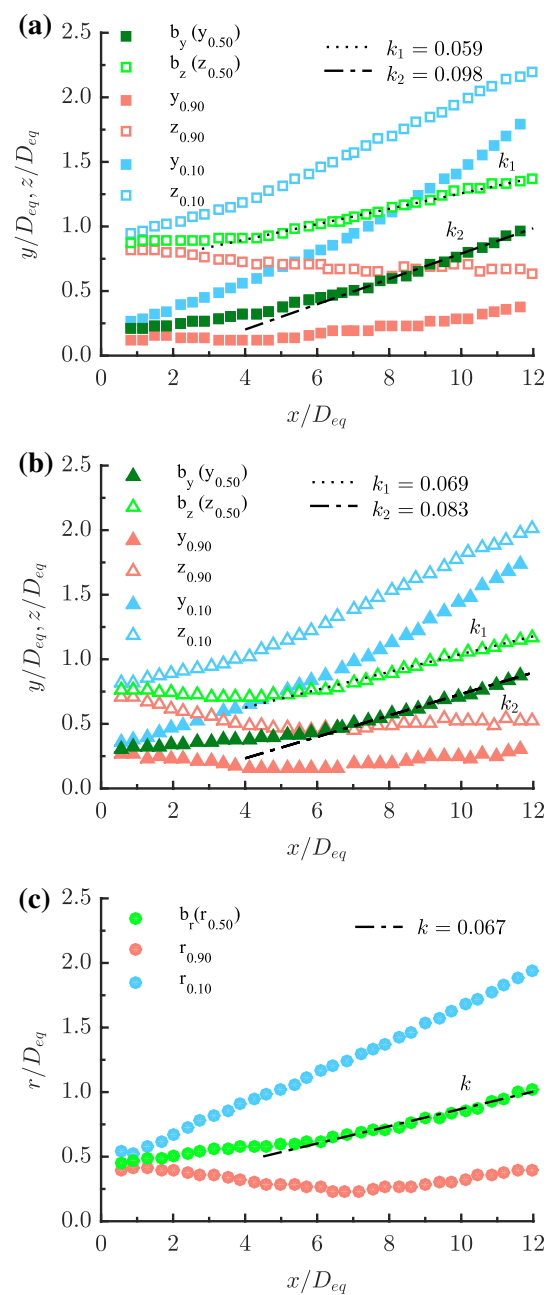
Fig. 7 Development of jet half-width, low-speed, and high-speed sides of the shear layer in the downstream direction for **a** *rectangular* **b** *elliptic* **c** *round* jets. For asymmetric jets, measurements in the major and minor axis planes are denoted as *open* and *closed symbols*, respectively. The growth rates for jet half-widths are denoted in the plots

curves for both the jets show slight inward growth. This is then followed by a positive linear outward growth for streamwise locations $x > 4D_{eq}$. Furthermore, for these downstream locations, jet half-width in the minor axis plane grows at a much faster rate compared to the major axis. This is especially true for the rectangular jet, where

the growth rate in the minor axis plane is more than 60% higher compared to the major. On the other hand, for the elliptic jet, this difference is not as dramatic, and the growth rate in the minor axis plane is approximately 20% higher compared to the major axis. Owing to these differences in growth rates, it appears that b_y curve will eventually approach or cross-over b_z at further downstream locations. However, as discussed in the context of Fig. 5, the current measurement domain shows no occurrence of axis-switching. In addition to jet half-width, both high- and low-speed sides of the shear layer also exhibit similar trends for both asymmetric jets. Shear layer bounds in the major and minor axis planes approach each other with increasing stream-wise distance. The low-speed side, or the outer bound of the shear layer, shows continual outward growth in both the planes. The high-speed side, on the other hand, shows continuous inward growth in the major plane. For the minor axis plane, this inner bound of shear layer grows inwards up until $x \approx 4D_{eq}$, followed by a gradual outward growth.

Figure 7c shows the shear layer bounds and half-width for the round jet. Jet half-width for the round jet is observed to grow at approximately the same rate as elliptic jet major axis. The outer bound of the shear layer has a continual outward growth, whereas the inner bound grows inwards for $x < 6D_{eq}$, followed by an outwards growth after the collapse of the potential core.

Finally, Fig. 8 compares shear layer thickness between asymmetric and round jets. The round jet has the thickest shear layer compared to both rectangular and elliptic jets. The major axis planes for both the asymmetric jets have higher shear layer thickness compared to their corresponding minor axis planes. The average shear layer growth rate for the round jet is approximately 0.125. The growth rates for the asymmetric jets are very similar, where the rectangular jet has average growth rates of 0.128 and 0.123 in the minor and major axis planes, respectively. Similarly, the elliptic jet exhibits an average growth rate of 0.126 and 0.123 in the minor and major axis planes, respectively. Moreover, by $x/D_{eq} \approx 12$ (not shown), the shear layer for all three nozzles begin to merge. It is apparent from these results that one should be careful while choosing the right parameters to define growth rates in asymmetric jets. Shear layer growth rate in this case, which is very similar for all three nozzles, is not a good representation of enhanced mixing in rectangular and elliptic jets.

3.2 Streamwise and spanwise vorticity

Mean asymmetric jet properties compared to the round jet so far revealed some variations in terms of velocity profiles, centerline decay, and jet spreading. However, for the given conditions, these observed changes are not very dramatic and the jets did not undergo axis-switching.
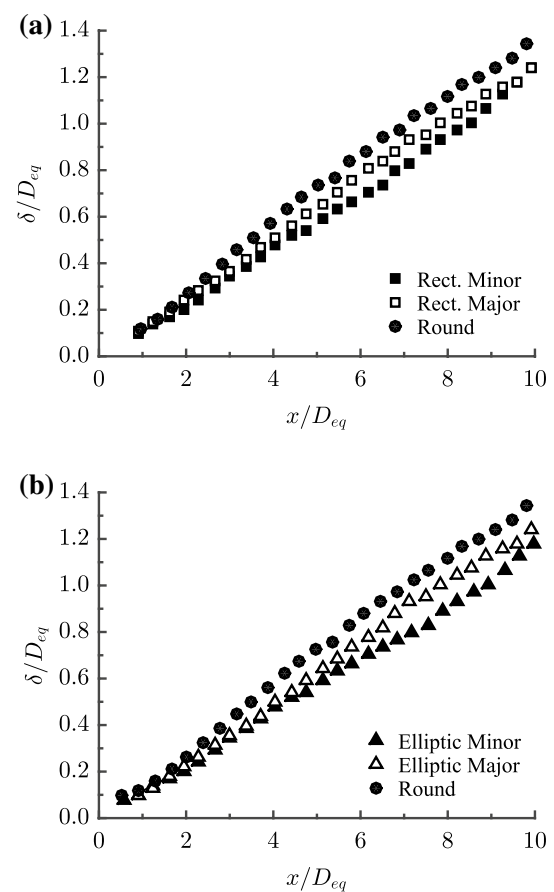
Fig. 8 Comparison of shear layer thickness for round jet with thicknesses in major and minor axis planes for **a** *rectangular* **b** *elliptic* jets

Moreover, the non-circular jets appear to be approaching axisymmetric state far downstream. These results agree with the findings of Zaman (1999), where the mass flux for non-axisymmetric jets was observed to be only slightly more compared to round nozzles at low- as well as high-subsonic conditions. In contrast, studies of Ho and Gutmark (1987) and Hussain and Husain (1989) showed much higher jet spreading with small aspect ratio nozzles at low speeds. Zaman (1999) pointed out that this difference likely arises from different initial flow conditions for the low Mach number jets used in these studies as well as the presence, or lack thereof, any streamwise structures at the jet exit. Moreover, as discussed in Sect. 1, shear layer dynamics in asymmetric jets, which lead to higher entrainment, spreading, and axis-switching, are primarily governed by the dynamics of spanwise and streamwise vorticity. In this section, we will present time averaged streamwise and spanwise vorticiy distribution for two asymmetric nozzles and compare them to the equivalent area round jet. The distribution of average vorticity values will be analyzed in relation to shear layer characteristics observed in Sect. 3.1.

Figure 9 presents normalized streamwise vorticity distribution for rectangular and elliptic jets at streamwise locations of x/D_{eq} of 1,2,3, and 5. Here, counter-clockwise sense of rotation for a vortex is considered positive. For the rectangular nozzle, the first plane, $x/D_{eq} = 1$, shows strong concentration of vorticity around the periphery of the nozzle exit. Even though concentrations of vorticity of opposite signs are observed in at least three of the four corner regions, these pairs do not appear very distinct. In the absence of any natural or artificial excitation, these vortices observed are likely formed due to upstream secondary flow within the nozzle (Prandtl's first kind of secondary flow) Bradshaw (1987). Further downstream at $x/D_{eq} = 2$, these vortex structures are observed to reorganize, where more distinct structures begin to appear at the corners. Moreover, two vortices of opposite signs along the shorter sides of the jet appear to come together and form a pair. This can be observed more clearly along the left shorter edge of the jet. By the next downstream plane, this pair seems to be dissipating rapidly. Moreover, at $x/D = 3$, one distinct vortex on each corner of the jet is observed, where two vortices on each end of the major axis have opposite sense of rotation. If two adjacent vortices of opposite signs were to form two counter-rotating pairs, such vortex pairs would be of outflow sense. This means that the sense of rotation of these vortices would eject the core flow out into the ambient from either side of the major axis (Zaman 1996). However, due to lack of strength and proximity, the two counter-rotating vortices do not form a pair and no 'outflow' of

the core jet is observed. The in-plane vectors (not shown here) do not reveal any 'outflow' effects but simply show entrainment of ambient air into the jet. For the final plane shown, $x/D_{eq} = 5$, the signature of four corner vortices is still somewhat visible, except they appear scattered and their strength is severely diminished.

The elliptic nozzle, Fig. 9b, shows similar trend. For the first observation plane, $x/D_{eq} = 1$, streamwise vorticity is observed to concentrate along the edge of the nozzle. For the subsequent downstream planes, $x/D = 2$ and 3, the vortices once again distribute mostly to corners or regions of smaller curvature. Unlike what was observed for the rectangular jet, no four distinct vortices of alternating signs are observed in four corners. Instead, in this case, the vortices along the nozzle edge appear randomly distributed. Once again by $x/D_{eq} = 5$, the strength of these structures appear highly diminished. Finally, Fig. 10 presents streamwise vorticity distribution for the round nozzle at one representative cross plane of $x/D_{eq} = 2$. As one would expect, this axisymmetric nozzle shows very low levels of streamwise vorticity that is randomly distributed and no distinct streamwise structures are observed.

Figure 11 presents spanwise vorticity distribution for the rectangular, elliptic, and round nozzles at streamwise locations of $x/D_{eq} = 2$, 4, and 6. For the rectangular and elliptical jets, spanwise vorticity for both major (ω_y) and minor (ω_z) axis planes are presented. Vorticity values are normalized using D_{eq} and U_j. For asymmetric jets, the x-axis is represented as non-dimensional variables $Y = (y - b_y)/D_{eq}$
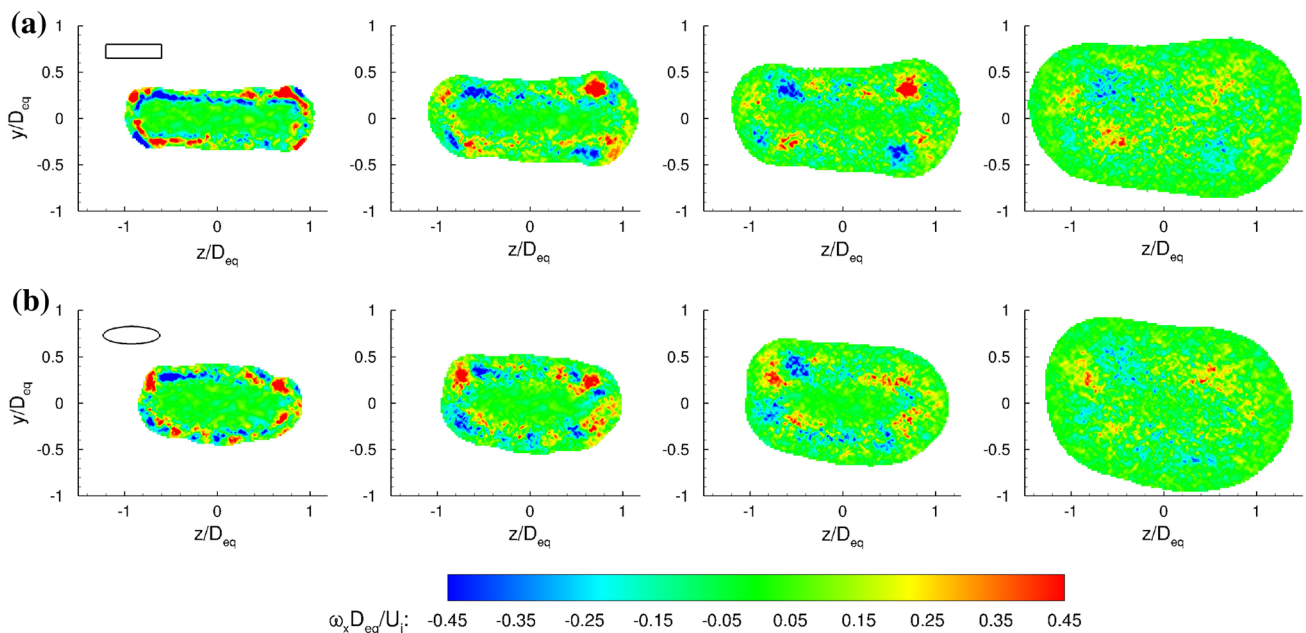
Fig. 9 Time averaged streamwise vorticity distribution for select cross planes, $x/D_{eq} = 1$, 2, 3 and 5 (*left to right*), for **a** *rectangular* **b** *elliptic* jets. The contour cut-off for the outer boundary of the vorticity field is defined by $0.05U_j$
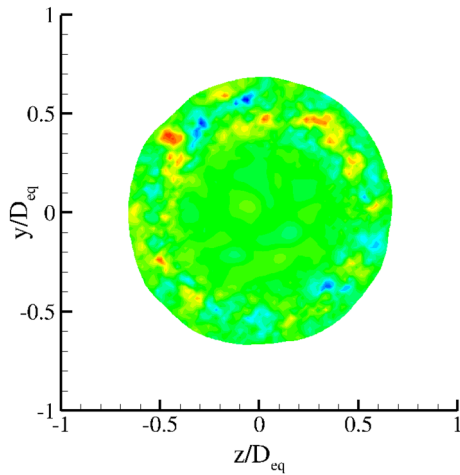
Fig. 10 Time averaged streamwise vorticity measurement for the round jet at $x/D_{eq} = 2$. The legend for this colored contour is the same as the one used in Fig. 9

and $Z = (z - b_z)/D_{eq}$ for the minor and major axes, respectively. For the round jet, $R = (r - b_r)/D_{eq}$ is used. Recall from Sect. 3.1 that b_y, b_z, and b_r are jet half-widths for minor axes, major axes, and round jet, respectively.

For the first location presented, it is clearly observed that spanwise vorticity is centered about the jet half-width for all three jets. The minor axis planes for the rectangular and elliptical nozzles have very similar magnitudes, which are only slightly higher than the values for the corresponding major axis planes. For subsequent downstream locations, the difference between the major and minor axes is further reduced and is observed to be within 10% of each other.

On comparing these results to round jet (ω_θ), one can notice a lower peak value, which is approximately 17% lower compared to the minor axes for the asymmetric jets, at $x/D_{eq} = 2$. For subsequent planes downstream, $x/D_{eq} = 3$ and 4, this difference between the round and

non-axisymmetric jets further increases. At $x/D_{eq} = 4$, peak spanwise vorticity for the round nozzle is as much as 27% lower compared to the asymmetric jets. A lower peak value for the round jet can be attributed to the thicker shear layer seen in Fig. 8. This difference in peak vorticity values begins to decrease by $x/D_{eq} = 5$, and by $x/D_{eq} = 6$, the distributions for all three nozzles appear nominally the same. Moreover, spanwise vorticity values for all three jets decline rapidly with increasing streamwise distance from the nozzle exit, where the peak vorticity is observed to shift slightly towards high-speed side of the shear layer.

Flow field results presented so far clearly suggest that vorticity dynamics for the given unexcited asymmetric jets at subsonic speeds do not favor axis-switching or more vigorous entrainment. For the given asymmetric jets, the presence of streamwise structures in the corner regions facilitates exchange of momentum and results in moderately enhanced entrainment. This is evidenced by shorter potential cores, higher growth rates of the jet half-width (see Sect. 3.1), and higher centerline turbulence (see Sect. 4). However, due to small size, low strength, and the lack of proximity between two vortices, no noticeable effect of induced velocity is observed in the shear layers of these asymmetric jets. As seen in Fig. 9, the undisturbed rectangular and elliptic jets begin to assume elliptic and round profiles, respectively, by $x/D_{eq} = 5$. This suggests that these jets are evolving and presumably approaching axisymmetric profile. Moreover, as discussed in Sect. 1, the dynamics of spanwise vorticity is also likely weaker at the present unexcited conditions.

4 Time averaged turbulence characteristics

This section presents representative turbulent quantities to further support the increased exchange of momentum or enhanced entrainment for the given non-circular nozzle
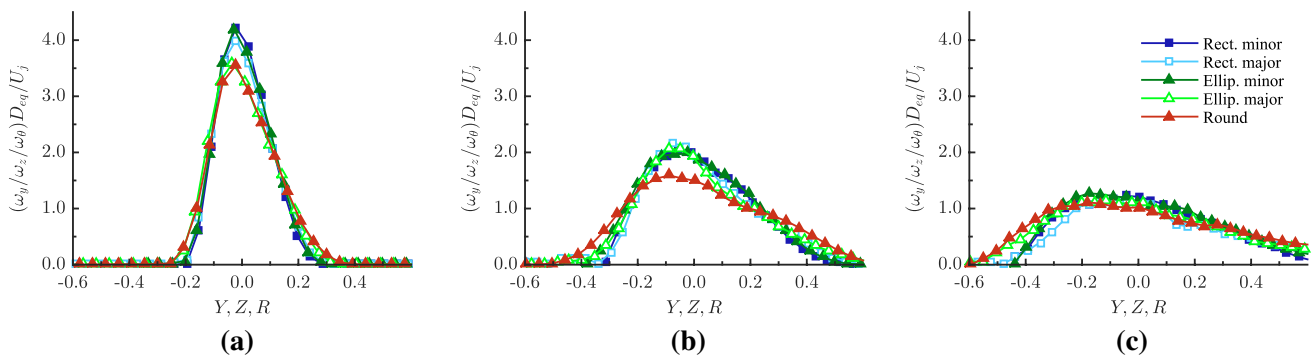
Fig. 11 Normalized spanwise vorticity values for rectangular, elliptical, and round nozzle at **a** $x/D_{eq} = 2$ **b** $x/D_{eq} = 4$, and **c** $x/D_{eq} = 6$. The non-dimensional variables are given by $Y = (y - b_y)/D_{eq}$, $Z = (z - b_z)/D_{eq}$, and $R = (r - b_r)/D_{eq}$. Here, b_y and b_z are corresponding jet half-widths for minor and major axis planes, respectively, for asymmetric jets. b_r is the half-width for the round jet
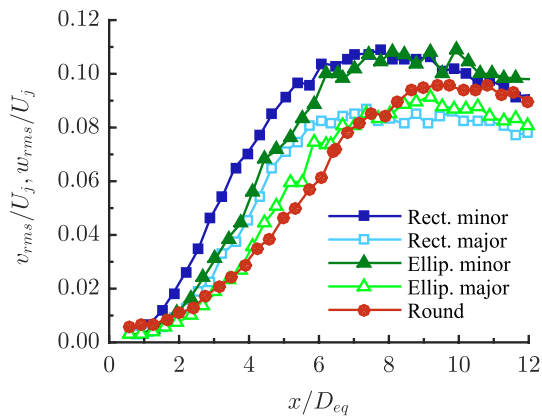
Fig. 12 Centerline transverse rms velocity distribution for *rectangular*, *elliptic*, and *round* jets. For the asymmetric jets, transverse turbulence intensity in the minor and major axes are given by v_{rms} and w_{rms}, respectively

geometries. Centerline distribution of root mean square (rms) values of transverse velocities and turbulent kinetic energy (TKE) is presented and compared with round jet values. This is followed by comparison of normalized transverse shear stress for different nozzle geometries.

Figure 12 compares the centerline distribution of transverse rms velocities for the rectangular, elliptic, and round nozzles. For the asymmetric jets, both v_{rms} and w_{rms} velocities along the minor (y-axis) and major (z-axis) axes, respectively, are presented. As expected, for both asymmetric nozzles, it is clear that the initial fluctuation levels are higher in the minor (y-axis) axis plane compared to the corresponding major axis (z-axis). Centerline rms fluctuations in the minor axis plane for both the jets peak at about 11% of U_j. On the other hand, the values for major axis peak between 8 and 9% of U_j. For the rectangular and elliptic jets, the differences between centerline rms velocity values in the major and minor axis planes is between 30 and 35% at $x \approx 5D_{eq}$.

Comparing the results for the two asymmetric nozzles, one can note that for a given streamwise location, rms values for the corresponding axes are slightly lower for the elliptic jet. Moreover, centerline distributions for the elliptic jet are observed to peak slightly downstream, where the rms values are marginally higher compared to the rectangular jet for far downstream locations ($x > 8D_{eq}$). The overall lower centerline fluctuations in the case of elliptic jet favors the longer potential core observed in the context of Fig. 6.

Finally, for the round nozzle, the centerline fluctuation values appear overall lower compared to both asymmetric jets. For instance, at $x = 5D_{eq}$, rms values for the round jet is approximately 50 and 40% lower compared to the values in minor axis planes for the rectangular and elliptic jets, respectively. The peak centerline value for this nozzle is

observed to be approximately 9.5% of U_j, where this peak occurs further downstream of the major axes for both the asymmetric jets. In addition, for $x > 7D_{eq}$, the rms values for the round jet exceed that of both the rectangular and elliptic major axis planes. Elevated levels of centerline fluctuations in the minor axis plane of the asymmetric jets suggest higher mixing compared to the major axis plane as well as the round jet. Section 5.1 will discuss azimuthal variation in the radiated noise levels for these nozzles, where the polar plane containing the minor axis of the jet exhibits higher noise levels in the downstream direction. Moreover, as subsequent acoustic spectra will show, increased turbulent fluctuations manifest themselves as elevated sound pressure levels at mid-to-high frequencies. This phenomena also known as 'high-frequency lift' is often observed with passive mixers such as tabs and chevrons (Simonich et al. 2001; Bridges et al. 2003).

Figure 13 shows centerline distribution of turbulent kinetic energy ($q^2 = \frac{1}{2}(\overline{u'^2} + \overline{v'^2} + \overline{w'^2})$) for three nozzles. Here, for the asymmetric jets, v' and w' values are extracted from the minor and major axis planes, respectively. Similarly, u' values extracted from either major or minor axis planes are nominally the same. For the round jet, v' values are used to represent radial velocity fluctuations, where TKE is given by $q^2 = \frac{1}{2}(\overline{u'^2} + \overline{2v'^2})$. As expected, for all upstream locations $x < 7D_{eq}$, the rectangular jet has the highest centerline TKE values, suggesting enhanced mixing. Moreover, these values increase rapidly and the peak assumes the most upstream position compared to elliptic or round jets. This is followed by a rapid dissipation in the downstream direction, resulting in fluctuation values that are the lowest of three nozzles for $x > 7D_{eq}$. This behavior of rectangular jet is in agreement with the shortest potential core measured for this nozzle. On the other hand, the round jet has overall lowest centerline TKE values for $x < 9D_{eq}$. Moreover, the increase is much more gradual compared to both the asymmetric jets and the values are observed to peak at the most downstream locations. Following the
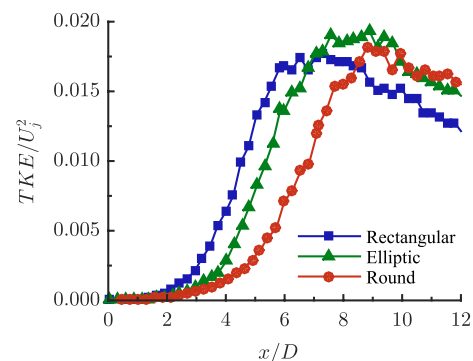
Fig. 13 Normalized centerline turbulent kinetic energy for *rectangular*, *elliptic*, and *round* jets

trends seen so far, centerline TKE values for the elliptic jet falls in between the rectangular and round nozzles for $x < 7D_{eq}$. The peak values occur slightly upstream of the round jet. Moreover, round and elliptic jets are observed to assume similar values for $x > 9D_{eq}$. This suggests near-axisymmetric state of the elliptic jet for far downstream locations.

Finally, normalized transverse Reynold's stress in the jet central plane is presented in Fig. 14 for select streamwise locations. For the asymmetric jets, shear stress values for minor (R_{xy}) and major (R_{xz}) axis planes both are shown in the same plot. Shear stress values are normalized with respect to the square of the local centreline velocity (U_c). For the rectangular jet, peak normalized shear stress start out fairly low and gradually increase in the downstream direction. In addition, transverse shear stress values in the minor axis plane are consistently higher compared to the major axis, where peak R_{xy} is as much as 27% higher than peak R_{xz} at $x = 6D_{eq}$. Towards the end of the measurement domain, $x \geq 10D_{eq}$, the stress values in the major and minor axis planes are observed to be comparable.

In case of the elliptic jet, similar trends are observed. However, differences in shear stress values between minor and major axis planes only become significant for $x > 4D_{eq}$. At $x = 6D_{eq}$, the peak stress value for the minor axis plane is observed to be approximately 25% higher compared to that of the major. When compared to the equivalent area rectangular jet, the elliptic jet appears to have lower peak transverse shear stress values in the minor axis plane. On the other hand, in the major axis plane, peak shear stress values for the elliptic jet exceed that of the rectangular jet for near nozzle locations ($x \leq 4D_{eq}$). However, for subsequent downstream locations $x > 4D_{eq}$, the rectangular jet maintains marginally higher values compared to the elliptic jet.

Figure 14c presents transverse (radial) shear stress distribution for the round jet. It can be observed that peak shear stress values for the round jet at $x/D_{eq} = 2$ are as much

as 40% higher compared to the minor axes planes for the asymmetric jets. Higher shear stress in regions closer to jet exit was also observed in the major axis plane for the elliptic jet in Fig. 14b. For subsequent downstream locations, $x/D_{eq} > 4$, normalized shear stress remains lowest for the round jet. For instance, for $x/D_{eq} = 6$, peak stress value for the round jet is approximately 36 and 26% lower compared to the values for rectangular and elliptic jet minor axis planes, respectively.

Results for time averaged turbulent quantities clearly show that asymmetric nozzles have increased centerline fluctuations compared to the round jet, signifying enhanced mixing. Overall, the rectangular jet appears to have the highest centerline rms velocities, turbulent kinetic energy as well as higher values for peak shear stresses. It is also evident from these results that the elliptic jet has properties that are intermediate between the two limiting nozzle geometries. This intermediate behavior is also evident in acoustic measurements where the OASPL of the elliptic jet falls between the round and rectangular jets (see Sect. 5). This further shows close relationship between modifications in turbulence distribution and resulting changes in acoustic radiation.

5 Jet acoustics

It is well known that large-scale coherent structures in the shear layer play a significant role in far-field noise radiation in supersonic as well as subsonic jets (Mollo-Christensen et al. 1964; Moore 1977; Tam et al. 2008; Morris 2009; Reba et al. 2009; Jordan and Colonius 2013). Therefore, one of the primary approaches to jet noise control is to manipulate the natural development and breakdown of these acoustically significant noise sources in the shear layer. Enhanced mixing properties of non-circular nozzle geometries are explored as cost-effective passive noise control technique that can potentially attenuate radiated
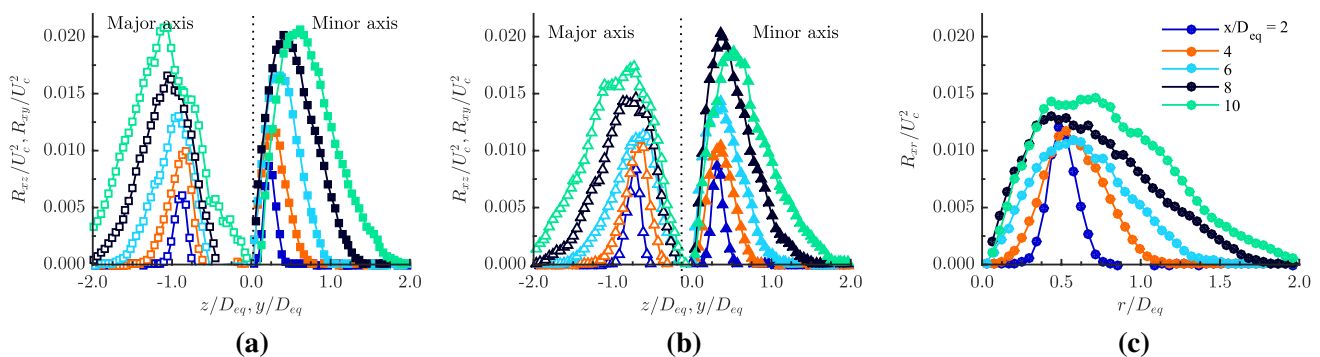
Fig. 14 Normalized transverse shear stress distribution at select streamwise locations for **a** *rectangular* **b** *elliptic*, and **c** *round* jets. For the asymmetric jets, transverse shear stress in both major (R_{xz}) and minor (R_{xy}) axis planes are presented

noise without severe performance penalties (Callaghan and Coles 1957; Seiner and Ponton 1992; Veltin and McLaughlin 2009; Bridges 2012). However, as discussed in Sect. 1, very few number of studies have been dedicated to measuring noise, especially from high-subsonic or shock-free supersonic asymmetric jets. In this section, we discuss far-field noise measurements to examine the effect of exit geometry changes on acoustic signatures of these jets. Once again, round jet measurements are used as a baseline and the effect of non-circular exits are assessed. We begin by presenting the OASPL for all three nozzles. Representative acoustic spectra at select polar angles are presented subsequently.

5.1 Directivity comparison

Figure 15a, b shows OASPL as a function of measured polar angles for the rectangular and elliptic nozzles, where directivity for both minor and major axis planes is included. The orientation of microphone arc with respect to the nozzle axes is discussed in Sect. 2.3.2. Moreover, OASPL values for the equivalent exit area round nozzle are also added, allowing comparison of overall radiation in the far field for three nozzle geometries. In addition, considering the cutoff frequency of the anechoic chamber, 300 Hz, OASPL values were integrated between $f = 314$ Hz and 50 kHz or $St = fD_{eq}/U_j = 0.027$ and 4.31, where f is the frequency.

OASPL plots demonstrate that the relative difference in noise level between round and two asymmetric jets, for the given Mach number, is not very significant. These comparisons are also summarized in Fig. 15c, where the difference in overall noise levels (ΔOASPL) between round and two asymmetric jets is presented for the measured polar angles. A positive value means that the OASPL for round jet exceeds that of the asymmetric jets. However, despite small differences in noise levels, not exceeding 1.5 dB, some interesting trends are observed which calls for further discussion. These trends reveal asymmetric radiation of these nozzles in the far-field.

In Fig. 15a and b, OASPL distributions for both rectangular and elliptic nozzles clearly show that for upstream and sideline angles, the minor axis plane of the jet exhibits a lower overall noise level compared to the major axis plane. A cross-over occurs at 100°, downstream of which the major axis plane provides consistent acoustic benefit with lower overall noise levels. For the rectangular jet, maximum difference between two planes occurs at $\theta = 140°$, where the minor axis plane exceeds the major axis noise levels by approximately 1.2 dB. For the elliptic jet, on the other hand, a maximum difference of 1.3 dB occurs at $\theta = 130°$. As discussed in Sect. 4, in the context of Fig. 12, directional nature of noise radiation observed for asymmetric jets is potentially due to observed differences
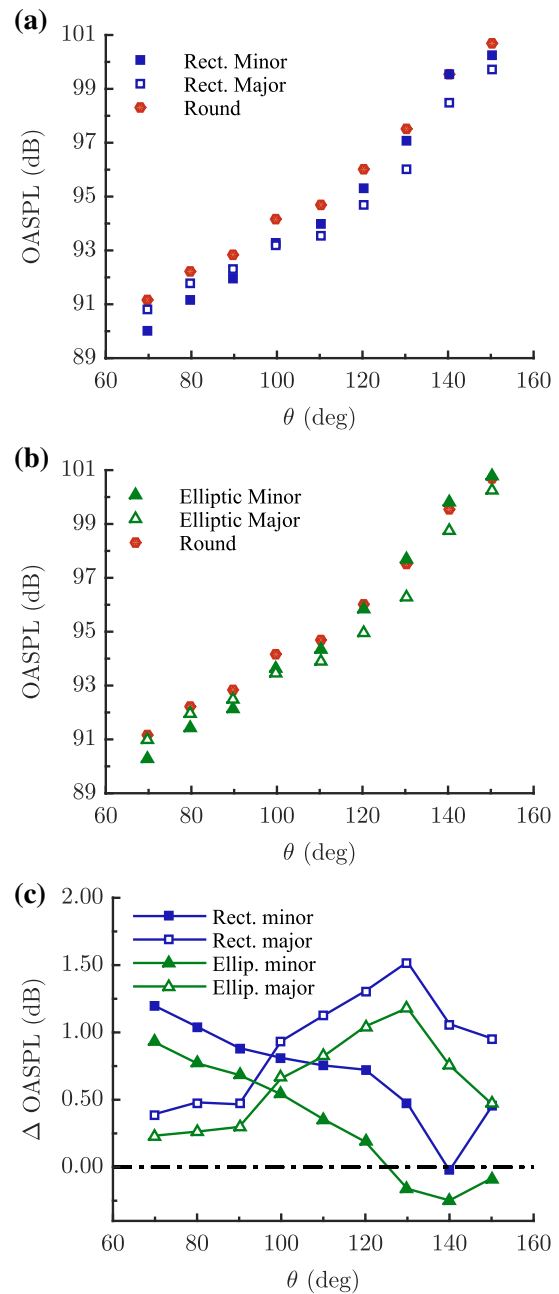
Fig. 15 OASPL distribution as a function of polar angle for **a** *rectangular* **b** *elliptic* jets. **c** differences in OASPL between round and asymmetric jets. A positive value denotes lower noise levels compared to round jet

in jet development in the major and minor axis planes. Elevated OASPL in the downstream direction for the minor axis plane perhaps results from higher mixing in this plane.

Figure 15c clearly shows differences in overall noise radiation between the round and asymmetric jets as a function of polar angle. For upstream and sideline angles, comparable OASPL values are observed for the round and major axes planes for both asymmetric

nozzles. However, for the downstream polar angles, the round nozzle becomes louder compared to the major axis planes for both rectangular and elliptic jets. By $\theta = 130°$, the round nozzle exceeds noise levels of the rectangular and elliptic jets by 1.5 and 1.2 dB, respectively. In contrast, for the minor axis planes, the differences in OASPL from the round nozzle are largest for the upstream angles. At 70°, the round jet is approximately 1.2 and 1 dB louder compared to the rectangle and elliptic jets, respectively. This difference decreases for downstream polar angles and the minor axis becomes comparable to (or even slightly louder than) the round jet for $\theta = 130°$–150°.

Overall these results suggest that the minor axis planes for the asymmetric nozzles dominate noise radiation in the downstream direction. Similar observations were made by Kinzie and McLaughlin (1999) for a 3:1 elliptic jet. When compared to an equivalent exit area round nozzle, the major axis orientation for the rectangular jet appears to provide the highest noise reduction for downstream angles. Also, it is evident that OASPL for the elliptic jet is intermediate between the values for rectangular and round jets. This was also discussed in the context of flow properties (Sects. 3, 4), where mean flow characteristics and turbulence distribution for elliptic jet exhibited properties that are intermediate between rectangular and round geometries.

Next, we examine acoustic spectra at select polar angles to investigate the contribution of different frequency ranges to the overall noise radiated for all three nozzles shapes and orientation axes.

5.2 Spectral characteristics

Figure 16 shows representative spectra at select polar angles for rectangular, elliptical, and round nozzles. Here, sound pressure level (SPL) is plotted as a function of Strouhal number, $St = fD_{eq}/U_j$. For both asymmetric nozzles, spectra in the major and minor axis planes reveal contributions of different frequency ranges at various polar angles measured from the jet axis. For lower polar angles (70° –90°), the noise levels appear overall very similar in both the planes. However, careful examination of the spectra reveal some differences which results in different far-field OASPL levels. Compared to minor, the major axis plane exhibits slightly lower noise levels for very low frequencies ($St_D < 0.1$) and slightly elevated noise levels at moderate frequencies. This observation is consistent for both asymmetric nozzles and results in a marginally higher OASPL for the major axis plane, as seen in Fig.15a and b for $\theta < 100°$.

As one progresses downstream in the direction of peak noise radiation, the minor axis plane becomes louder and exceeds SPL for major axis plane after a certain 'cross-over' Strouhal number. Interestingly, as the spectral peak (St_{peak}) shifts to lower frequencies with increasing downstream angle, this 'cross-over' is also observed to occur at lower frequencies. This spectral behavior demonstrates that higher OASPL observed for $\theta > 100°$ in the polar plane containing minor axis (see Fig. 15a, b) is primarily due to increased SPL at moderate to high frequencies. For instance, when compared to the major axis plane, the spectra for the minor plane for 130°, for both rectangular and elliptic nozzles clearly show an increase of as much as 5 dB

Fig. 16 Acoustic spectra for representative polar angles showing SPL for **a** *rectangular* **b** *elliptic* jets. Spectra for the equivalent exit area round jet are added for comparison
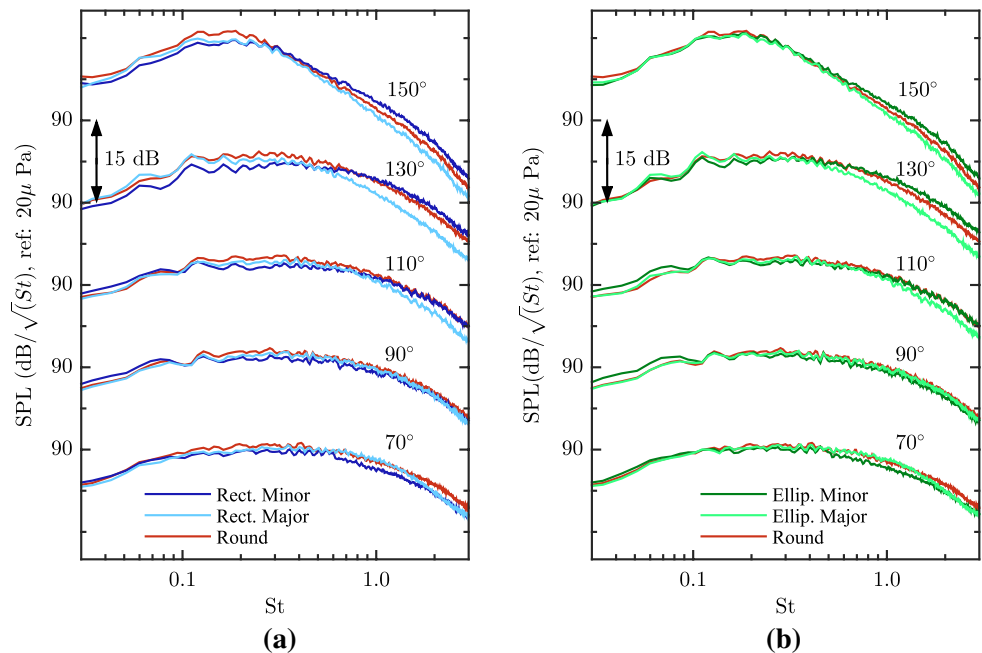
for $St > 0.5$. As discussed in Sect. 4, this observed increase in high-frequency noise is potentially due to enhanced mixing in the minor axis plane. Increased mixing in this axis was also demonstrated by mean flow profiles, higher jet half-width growth rates, and increased rms fluctuations in the jet centerline. In addition, for $\theta \geq 130°$, rectangular jet spectra shows a noticeable reduction in SPL for lower frequencies in the minor axis plane. For the elliptic jet, on the other hand, the low frequency levels remain fairly similar in both the planes.

Comparing the rectangular jet sound field to an equivalent area round jet, one can note that for lower polar angles, $\theta = 70°$–$100°$, round nozzle noise levels are marginally higher than the minor axis plane across the entire spectrum, except at very low frequencies ($St < 0.1$). However, the most significant differences are observed for downstream angles ($\theta \geq 130°$), where the minor axis plane for the rectangular jet exhibits reduced low frequency noise compared to the round jet. A cross-over occurs after which SPL for the minor axis plane is consistently higher compared to the round jet. This cross-over is once again observed to shift to lower Strouhal numbers for increasing downstream angles. Overall, for downstream polar angles ($\theta > 130°$), the minor axis plane for the rectangular jet exhibits highest noise levels at moderate to high frequencies, potentially resulting from increased mixing. However, for the same downstream angles, the minor plane radiates lowest noise levels at low frequencies ($St < 0.3$). This suggests that low frequency noise sources are comparatively weaker in the minor axis plane of a rectangular jet. As discussed in Sect. 4, several studies involving passive mixers have demonstrated similar reduction of low frequency noise with noise augmentation at high-frequencies, known as high-frequency lift.

Spectra for major axis plane for the rectangular jet are comparable to the round jet for upstream and sideline angles ($\theta < 90°$). However, the difference between them observably increases for downstream polar angles, where the noise levels for rectangular major axis plane remain consistently lower compared to the round jet for $St > 0.2$.

The elliptic jet shows similar spectral trends when compared to the round jet, except the observed differences are somewhat smaller. The minor axis plane for the elliptic jet once again shows increased moderate to high-frequency noise for downstream angles. Reduction in low frequency noise, observed in the case of rectangular jet minor axis, is not seen here. Similar to the rectangular jet, the major axis plane for elliptic jet assumes consistently lower noise levels compared to the round jet for downstream polar angles.

Overall, some interesting trends that reflect the effect of nozzle asymmetry in the radiated noise field are observed. Upon examining the spectral properties, it can be concluded that the minor axis plane radiates highest overall noise levels in the downstream direction, where these acoustic contributions are primarily from moderate- to high-frequency sources. This is presumably due to higher fluctuation levels in the minor axes as well as the possible dominance of flapping mode, as discussed by Kinzie and McLaughlin (1999). The lowest noise levels in the downstream directions are that of rectangular jet major axis plane. This existence of 'loud' and 'quite' planes agree with the results of Seiner and Ponton (1992), Kinzie and McLaughlin (1999) and Goss et al. (2009). This preferential radiation characteristic, especially when higher overall difference exists between major and minor axis planes, can be exploited in aircraft exhausts to direct quieter plane towards noise sensitive areas. Compared to the round jet, the overall reduction in noise levels due to nozzle asymmetry in the downstream direction is limited to 1.5 dB. Spectral distribution shows SPL difference of as much as 3.5 dB between the round and rectangular major axis for the downstream angle of 130°. Therefore, it is evident that for the given operating and nozzle conditions, these asymmetric jets only provide nominal acoustic benefit in the downstream angles when compared to the round jet. Similar results were obtained by Tam and Zaman (2000), who compared sound field from subsonic rectangular and elliptic jets. However, despite small reductions, the asymmetric nozzle geometries tested still show promise in attenuating radiated noise. Acoustic measurements at various pertinent Mach number and temperature conditions are necessary to fully explore the potential of these asymmetric nozzle geometries as passive noise control technique.

6 Concluding remarks

Flow and acoustic characteristics of converging rectangular (AR = 4) and elliptic (AR = 2.5) nozzles were presented. An equivalent exit area round nozzle was used as a baseline case for comparison of results. The jets were operated at nominally isothermal conditions and a Mach number of 0.9. Time average flow field results obtained using planar and stereoscopic PIV showed the influence of nozzle exit geometry in the downstream evolution of the jets. In general, the elliptic jet demonstrated intermediate flow properties between the rectangular and circular extremes.

Both rectangular and elliptic jets exhibited shorter potential core and faster growth rate of jet half-width, suggesting enhanced mixing compared to the round jet. Despite higher shear layer growth rates in the minor axes compared to the major, no evidence of axis-switching was observed for the given measurement domain. Cross plane measurements revealed the presence of relatively weaker streamwise vortices in the corner regions or edges of the jet profile. These vortices facilitate the transport of momentum and are responsible for moderately enhanced growth rates of the

asymmetric jet shear layer. However, due to low strength and lack of proximity between two vortex pairs, no effect of induced velocity was observed. The undisturbed jet profiles for the rectangular and elliptic jets were observed to evolve into elliptic and round shapes, respectively, in the downstream direction. Centerline turbulent fluctuations were overall higher for rectangular and elliptic jets. Except for near nozzle locations, normalized peak transverse shear stress values were also greater for the rectangular and elliptic jets. Furthermore, enhanced fluctuation in the minor axis plane of these asymmetric jets was evidenced by higher values for rms velocities and shear stresses.

Far-field acoustic measurements of the non-circular jets showed that the minor axis plane was louder compared to the major in the downstream direction. Acoustic spectra for downstream polar angles revealed that this increase in OASPL in the minor axis plane is mostly contributed by moderate to high-frequency sources. This is potentially due to enhanced mixing by the streamwise structures. When compared to the round jet, major axis planes of the asymmetric jets were observed to provide modest acoustic benefit in the peak noise radiation direction. Even though the differences in OASPL from the round jet was not as significant for the given jet conditions, these asymmetric jets still showed promise in attenuating radiated noise in the far-field. A comprehensive database of flow field and noise characteristics for asymmetric jets at high subsonic and supersonic speeds as well as elevated temperature conditions is necessary to further explore the potential of these nozzles in future aircraft propulsion systems.

References

Alkislar M, Krothapalli A, Lourenco L (2003) Structure of a screeching rectangular jet: a stereoscopic particle image velocimetry study. J Fluid Mech 489:121–154

Bradshaw P (1987) Turbulent secondary flows. Annu Rev Fluid Mech 19(1):53–74

Bridges J, Wernet M, Brown C (2003) Control of jet noise through mixing enhancement. NASA Report No NASA/TM 212335

Bridges JE (2012) Acoustic measurements of rectangular nozzles with bevel. National Aeronautics and Space Administration, Glenn Research Center, Fairview Park

Bridges JE, Wernet MP (2015) Turbulence measurements of rectangular nozzles with bevel. In: 53rd AIAA Aerospace sciences meeting, p 0228

Callaghan EE, Coles WD (1957) Far noise field of air jets and jet engines. NACA report 1329

Capone FJ (1975) Supercirculation effects induced by vectoring a partial-span rectangular jet. J Aircr 12(8):633–638

Coles WD (1959) Jet-engine exhaust noise from slot nozzles, vol 60. National Aeronautics and Space Administration, Washington, DC

Craft J, Upadhyay P, Worden TJ, Alvi FS (2016) Characterization and validation of an anechoic facility for high-temperature jet noise studies. In: 46th AIAA fluid dynamics conference, p 3800

Goss AE, Veltin J, Lee J, McLaughlin DK (2009) Acoustic measurements of high-speed jets from rectangular nozzle with thrust vectoring. AIAA J 47(6):1482–1490

Grinstein FF (2001) Vortex dynamics and entrainment in rectangular free jets. J Fluid Mech 437:69–101

Gutmark E, Grinstein F (1999) Flow control with noncircular jets 1. Annu Rev Fluid Mech 31(1):239–272

Hiley P, Wallacet H, Booz D (1976) Nonaxisymmetric nozzles installed in advanced fighter aircraft. J Aircr 13(12):1000–1006

Ho C, Gutmark E (1987) Vortex induction and mass entrainment in a small-aspect-ratio elliptic jet. J Fluid Mech 179:383–405

Husain HS, Hussain F (1993) Elliptic jets. Part 3. Dynamics of preferred mode coherent structure. J Fluid Mech 248:315–361

Hussain F, Husain H (1989) Elliptic jets. Part 1. Characteristics of unexcited and excited jets. J Fluid Mech 208:257–320

Jordan P, Colonius T (2013) Wave packets and turbulent jet noise. Annu Rev Fluid Mech 45:173–195

Kim JH, Samimy M (1999) Mixing enhancement via nozzle trailing edge modifications in a high speed rectangular jet. Phys Fluids (1994-present) 11(9):2731–2742

Kinzie KW (1995) Aeroacoustic properties of moderate reynolds number elliptic and rectangular supersonic jets. PhD Thesis, Pennsylvania State University

Kinzie KW, McLaughlin DK (1999) Aeroacoustic properties of supersonic elliptic jets. J Fluid Mech 395:1–28

Krothapalli A, Baganoff D, Karamcheti K (1981) On the mixing of a rectangular jet. J Fluid Mech 107:201–220

Mollo-Christensen E, Kolpin MA, Martuccelli JR (1964) Experiments on jet flows and jet noise far-field spectra and directivity patterns. J Fluid Mech 18(02):285–301

Moore C (1977) The role of shear-layer instability waves in jet exhaust noise. J Fluid Mech 80(02):321–367

Morris PJ (2009) A note on noise generation by large scale turbulent structures in subsonic and supersonic jets. Int J Aeroacoust 8(4):301–315

Morris PJ, Bhat TR (1995) The spatial stability of compressible elliptic jets. Phys Fluids (1994-present) 7(1):185–194

Papamoschou D, Roshko A (1988) The compressible turbulent shear layer: an experimental study. J fluid Mech 197:453–477

Quinn W (1994) Development of a large-aspect-ratio rectangular turbulent free jet. AIAA J 32(3):547–554

Reba R, Simonich J, Schlinker R (2009) Sound radiated by large-scale wave-packets in subsonic and supersonic jets. AIAA Pap 3256:11–13

Seiner JM, Ponton MK (1992) Supersonic acoustic source mechanisms for free jets of various geometries. In: In AGARD, Combat Aircraft Noise 12 p (SEE N93-10666 01-71), vol 1

Sfeir A (1976) The velocity and temperature fields of rectangular jets. Int J Heat Mass Transf 19(11):1289–1297

Sfeir A (1979) Investigation of three-dimensional turbulent rectangular jets. AIAA J 17(10):1055–1060

Sforza P, Steiger M, Trentacoste N (1966) Studies on three-dimensional viscous jets. AIAA J 4(5):800–806

Shih C, Krothapalli A, Gogineni S (1992) Experimental observations of instability modes in a rectangular jet. AIAA J 30(10):2388–2394

Simonich J, Narayanan S, Barber T, Nishimura M (2001) Aeroacoustic characterization, noise reduction, and dimensional scaling effects of high subsonic jets. AIAA J 39(11):2062–2069

Tam C, Zaman K (2000) Subsonic jet noise from nonaxisymmetric and tabbed nozzles. AIAA J 38(4):592–599

Tam C, Golebiowski M, Seiner J (1996) On the two components of turbulent mixing noise from supersonic jets. In: Aeroacoustics conference, p 1716

Tam CK, Viswanathan K, Ahuja K, Panda J (2008) The sources of jet noise: experimental evidence. J Fluid Mech 615:253–292

Trentacoste N, Sforza P (1968) Some remarks on three-dimensional wakes and jets. AIAA J 6(12):2454–2456

Tsuchiya Y, Horikoshi C (1986) On the spread of rectangular jets. Exp Fluids 4(4):197–204

Valentich G, Upadhyay P, Kumar R (2016) Mixing characteristics of a moderate aspect ratio screeching supersonic rectangular jet. Exp Fluids 57(5):1–14

Valentich GM (2016) Flow field and acoustic characterization of non-axisymmetric jets. Master's Thesis, Florida State University

Veltin J, McLaughlin D (2009) Flow field and acoustic measurements of rectangular supersonic jets. 47th AIAA Aerospace Sciences Meething and Exhibit

Viswanath K, Johnson R, Corrigan A (2016) Noise characteristics of a rectangular vs circular nozzle for ideally expanded jet flow. AIAA Pap 1638:2016

Wieneke B (2015) PIV uncertainty quantification from correlation statistics. Meas Sci Technol 26(7):074002

Zaman K (1996) Axis switching and spreading of an asymmetric jet: the role of coherent structure dynamics. J Fluid Mech 316:1–27

Zaman K (1999) Spreading characteristics of compressible jets from nozzles of various geometries. J Fluid Mech 383:197–228

Zaman K (1994) Effect of 'delta tabs' on mixing and axis switching in jets from asymmetric nozzles, vol 106450. National Aeronautics and Space Administration, Washingdon, DC